Received May 2000
Revised September 2000
Accepted September 2000

Numerical study of periodically turbulent flow and heat transfer in a channel with transverse fin arrays

Z.X. Yuan
College of Environment and Energy Engineering, Beijing Polytechnic University, Beijing, China

Keywords *Turbulence, Heat transfer, Channels, Fins*

Abstract *A numerical study has been conducted for the characteristics of the periodically fully developed turbulent flow and heat transfer in a channel with transverse opposite-positioned fins. The Reynolds number range is 2×10^4 to 7×10^4. K-ε model and wall function method were adopted during the calculation. The influence of the thermal boundary condition of the fin to the heat transfer has been verified. For the studied configuration the prominent feature that differs from the similar laminar heat transfer is the phenomenon of secondary peak of the Nusselt number distribution. Assessment of heat transfer enhancement under the constraint of the same pump power reveals that the effect of the configuration of the relative fin height, e/H, equal to 0.1 is superior to those of e/H equal to 0.15 and 0.2. Comparing with the results of the channel with rod disturbances, the studied configuration possesses nearly the same heat transfer enhancement effect. Transient simulations to cases with big fin have also been conducted to assure the validity of the steady algorithm.*

Nomenclature

c = turbulent constants, Table I
De = equivalent diameter
e = fin height
f = friction factor, equation (23)
h = heat transfer coefficient, equation (19)
H = half channel height
k = thermal conductivity of air
K = turbulent kinetic energy
M = mass flow rate
N = pump power, equation (24)
Nu(x) = local Nusselt number, equation (21)
Nu = cycle-averaged Nusselt number
p = fluid pressure
P = pitch of fin array
Pr = Prandtl number
Re = Reynolds number
S = turbulent source term, equations (11-14)
Sh = Sherwood number
T = fluid temperature
u = fluid velocity in x-direction
$\bar{u}$ = cross-sectional averaged velocity
v = fluid velocity in y-direction
x,y = rectangular coordinate

Greek symbols

Γ = generalized diffusion coefficient, equations (7- 10)
ε = turbulent dissipation rate
μ = viscosity
υ = kinematic viscosity
ρ = air density
σ = turbulent constants, Table I

Subscripts

b = bulk average
o = smooth channel
p = first inner node from wall
t = turbulent
w = wall

International Journal of Numerical Methods for Heat & Fluid Flow, Vol. 10 No. 8, 2000, pp. 842-861.

Introduction

Use of artificial roughened surface is a common method to enhance heat transfer in channel flows. The disturbances inside the channel may have various types. The height of the disturbances is usually 1-5 percent of the hydraulic diameter. Though different types of channel cross section can occur in actual engineering, it is supposed that the rectangular channel has the most extensive application in the fields of refrigeration, compact heat exchanger and electronic board cooling, etc. As the extension of rectangular type, the enhanced configuration of parallel-plate channel with disturbing rods or short fins has been reported a lot in open literature. Chen and Huang (1991) studied the forced laminar convection in parallel-plate channels with transverse fin arrays numerically. In general, the in-line arrangement behaves ineffectively due to the remarkable flow recirculation covering the wall surfaces. Similar channels with rod disturbances instead of fins were numerically investigated by Yuan and Tao (1998) in the Reynolds number range of 50-700, concluding that the Nusselt number can reach four-fold of a smooth channel at the same condition but with the penalty of much greater pressure drop. Sparrow and Tao (1983, 1984) measured the turbulent characteristics of the above rod channel symmetrically and asymmetrically deployed disturbances. The symmetric disturbances yielded significantly increased transfer coefficients up to a factor of three compared with a corresponding disturbance-free duct, and exceeded those of asymmetric cases. The present author and others also studied experimentally the duct with periodic rectangular fins along the main flow direction (Yuan *et al.*, 1998) and the duct with winglet fins (Yuan *et al.*, 1999). They can both increase heat transfer largely comparing with smooth duct.

A lot of reports for numerical simulation of laminar flow and heat transfer can be found in open literature. For example, Hong *et al.* (1991) investigated the characteristics of laminar separation and reattachment of flow in the channel with one ribbed wall. Xin and Tao (1988) reported the numerical prediction of periodically fully developed laminar flow and heat transfer in wavy channels.

The numerical model for turbulent flow and heat transfer has been developing by now. As one of complex heat transfer configurations the periodically disturbed channel can not be said to reach perfect numerically studied status, especially in the range of turbulent flow. Among many turbulent models, K-ε model is relatively mature and widely applied. Using this model, Pourahmadi and Humphrey (1983) studied the curved channel flow. Amano *et al.* (1987) and Amano (1985) also used K-ε model to compute the turbulent heat transfer in a periodically wall-corrugated channel successfully.

Different from the case of laminar flow, the simulation of turbulent flow requires much finer grid division. At this point the configuration studied by Sparrow and Tao (1984) may have some difficulties in the grid division because of the presence of the rod disturbances on the duct wall, and probably be suitable to be dealt with body-fitted coordinate. The present work is the preliminary study for that configuration. The main objectives of the present investigation for the channel with transverse fin arrays are:

(1) to study the details of turbulent flow and heat transfer in one cycle, determining the local Nusselt number distribution and average characteristics of the friction and heat transfer coefficient;

(2) to compare the numerical results of the present enhanced configuration with those of similar channels with rod disturbances experimented by Sparrow and Tao (1984).

Mathematical and numerical models

Configuration and solution domain

The scheme of the enhanced configuration and solution domain is shown in Figure 1. In accordance with the experiments of Sparrow and Tao (1984), opposite plate fins are deployed on top and bottom walls in the present study. On the other hand, the purpose of using disturbances in such kind of channels is mainly to increase the turbulence intensity in the wall-vicinity region and to reduce the thickness of the viscous sublayer, not to enlarge the heat transfer area with the disturbances. So in the present study the plate fin was basically treated as adiabatic body and its thickness was assumed to be zero, but the efficiency of the fin with the same temperature as the main wall has been checked for a typical case.

Governing equations

With K-ε two-equation model the two-dimensional steady turbulent flow and heat transfer are described as (without consideration of volumetric force):

$$\frac{\partial u}{\partial x}+\frac{\partial v}{\partial y}=0 \tag{1}$$

$$\rho(u\frac{\partial u}{\partial x}+v\frac{\partial u}{\partial y})=\frac{\partial}{\partial x}(\Gamma\frac{\partial u}{\partial x})+\frac{\partial}{\partial y}(\Gamma\frac{\partial u}{\partial y})+S_u \tag{2}$$

$$\rho(u\frac{\partial v}{\partial x}+v\frac{\partial v}{\partial y})=\frac{\partial}{\partial x}(\Gamma\frac{\partial v}{\partial x})+\frac{\partial}{\partial y}(\Gamma\frac{\partial v}{\partial y})+S_v \tag{3}$$

$$\rho(u\frac{\partial K}{\partial x}+v\frac{\partial K}{\partial y})=\frac{\partial}{\partial x}(\Gamma_K\frac{\partial K}{\partial x})+\frac{\partial}{\partial y}(\Gamma_K\frac{\partial K}{\partial y})+S_K \tag{4}$$

$$\rho(u\frac{\partial \varepsilon}{\partial x}+v\frac{\partial \varepsilon}{\partial y})=\frac{\partial}{\partial x}(\Gamma_\varepsilon\frac{\partial \varepsilon}{\partial x})+\frac{\partial}{\partial y}(\Gamma_\varepsilon\frac{\partial \varepsilon}{\partial y})+S_\varepsilon \tag{5}$$

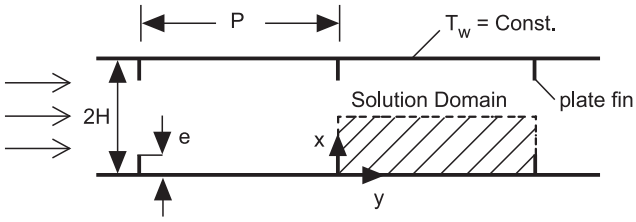

Figure 1.
Channel scheme and solution domain

$$\rho(u\frac{\partial T}{\partial x}+v\frac{\partial T}{\partial y})=\frac{\partial}{\partial x}(\Gamma_T\frac{\partial T}{\partial x})+\frac{\partial}{\partial y}(\Gamma_T\frac{\partial T}{\partial y}) \tag{6}$$

The diffusion coefficients and source items in above equations are

$$\Gamma=\mu+\mu_t \tag{7}$$

$$\Gamma_K=\mu+\mu_t/\sigma_K \tag{8}$$

$$\Gamma_\varepsilon=\mu+\mu_t/\sigma_\varepsilon \tag{9}$$

$$\Gamma_T=\mu/\mathrm{Pr}+\mu_t/\sigma_T \tag{10}$$

$$S_u=-\frac{\partial p}{\partial x}+\frac{\partial}{\partial x}(\Gamma\frac{\partial u}{\partial x})+\frac{\partial}{\partial y}(\Gamma\frac{\partial v}{\partial x}) \tag{11}$$

$$S_v=-\frac{\partial p}{\partial y}+\frac{\partial}{\partial x}(\Gamma\frac{\partial u}{\partial y})+\frac{\partial}{\partial y}(\Gamma\frac{\partial v}{\partial y}) \tag{12}$$

$$S_K=G-\rho\varepsilon \tag{13}$$

$$S_\varepsilon=\frac{\varepsilon}{K}(c_1G-c_2\rho\varepsilon) \tag{14}$$

$$G=\mu_t\left\{2\left[\left(\frac{\partial u}{\partial x}\right)^2+\left(\frac{\partial v}{\partial y}\right)^2\right]+\left(\frac{\partial u}{\partial y}+\frac{\partial v}{\partial x}\right)^2\right\} \tag{15}$$

The turbulent viscosity μ_t is decided by Prandtl-Kolmogrov formula

$$\mu_t=c_\mu\rho K^2/\varepsilon \tag{16}$$

The turbulent constants in above equations were adopted in accordance with those of Serag-Eldin and Spalding (1979), Chieng and Launder (1980) and Farouk and Guceri (1982). They are shown in Table I.

Near-wall model of the K-ε and grid system

The finite volume approach incorporated with SIMPLE algorithm and the power-law scheme (Patankar, 1981) was adopted to discretize and solve the governing equations. Since the turbulence model employed in this computation is the high Reynolds number form, it is necessary to introduce the "wall-function" approach (Launder and Spalding, 1974) into the normal procedure for turbulence computation for the wall adjacent numerical cells. The evaluation of

c_μ	c_1	c_2	σ_K	σ_ε	σ_T
0.09	1.44	1.92	1.0	1.3	0.9

Table I. Turbulent constants in the governing equations

the ε in the wall-vicinity region must be treated specially. ε_p is decided as follows

$$\varepsilon_p = \frac{c_\mu^{3/4} K_p^{3/2}}{0.4 y_p} \tag{17}$$

According to the wall-function it demands that the first node point p lie in the fully turbulent region, satisfying $11.5 \leq y_p^+ \leq 400$ ($y_p^+ = y_p c_\mu^{1/4} K_p^{1/2} / \upsilon$). On the other hand, since there exists great velocity gradient in the near-wall region, very fine grid is needed to obtain accurate computational result. Thus, it is necessary to take non-uniform grid system to divide the computational domain in y-direction. In the study, the first cell neighboring the wall was kept large enough to meet $y_p^+ \geq 11.5$. Starting from the second cell the grid changed from fine to coarse gradually, with a relaxing factor equal to 1.07. The grid in x-direction is uniformly divided. A careful check for the grid-independence of the numerical solution has been made to ensure the accuracy and validity of the numerical scheme. For this purpose, five grid systems from 70 × 40 to 250 × 150 have been tested, as shown in Table II. It is found that for Re = 4×10^4 the relative error in the friction factor between the solutions of 200 × 120 and 250 × 150 is 0.9 percent and in Nusselt number is 0.5 percent. In view of saving computation time a grid system of 200 × 120 is adopted typically in the computation.

The handling of the boundary conditions for the inlet and outlet of the solution domain has been thoroughly discussed in the previous work of Yuan *et al.* (1998). Therefore they will not be repeated here. A point worthy to note is the boundary condition in the solid wall for the K equation. Following Launder and Spalding (1974), $(\partial K/\partial y)_w = 0$ has been adopted in the computation, so it is adiabatic condition in the solid wall for the K equation.

Computations of Nusselt number and friction factor

Reynolds number is defined as

$$Re = \frac{\bar{u} \cdot D_e}{\nu} \tag{18}$$

where $\bar{u}$ represents the longitudinal velocity averaged in the cross-section without fin. The hydraulic diameter is $D_e = 4H$. In the main flow direction the local heat transfer coefficient h(x) is calculated as

Table II.
The tested results of grid system (Re = 4×10^4)

Grid number	74 × 40	120 × 60	150 × 90	200 × 120	250 × 150
Nu	276.9	283.3	277.7	255.8	257.1
f	0.1551	0.2235	0.2312	0.2366	0.2344

$$h(x) = k_t(x)\frac{T_w - T_p(x)}{y_p}\cdot\frac{1}{T_w - T_b(x)} \tag{19}$$

where k_t is the turbulent thermal conductivity decided by wall function method. The subscript "p" indicates the first inner node from the solid wall. Considering that the computation is confined in one cycle and the difference between T_w and bulk temperature $T_b(x)$ does not vary largely along the main flow direction, the cycle-averaged heat transfer coefficient, $\bar{h}$, can be decided as follows

$$\bar{h} = \frac{1}{P}\int_0^P h(x)dx \tag{20}$$

Corresponding to h(x) and $\bar{h}$ the local Nusselt number, Nu(x), and cycle-averaged Nusselt number, Nu, are

$$Nu(x) = \frac{h(x)\cdot D_e}{k} \tag{21}$$

$$Nu = \frac{\bar{h}\cdot D_e}{k} \tag{22}$$

where k is the conductivity of the fluid. The cycle-averaged friction factor is defined by Darcy definition

$$f = \frac{\Delta p}{\frac{P}{D_e}\cdot\frac{\rho\bar{u}^2}{2}} \tag{23}$$

where $\triangle$p is the pressure drop of the cycle, given by the numerical results. All physical values of the fluid are decided by the air.

Results and discussion

By the open literature (e.g. Chen and Huang, 1991; Sparrow and Tao, 1984) the relative pitch, P/H, and the relative height, e/H, of the disturbances are main geometric parameters to influence the enhancement effect of the channel. In this study the e/H changes from 0.10 to 0.20 and P/H from 1.0 to 5.0. The Reynolds number is in the range of 2×10^4~7×10^4.

Flow pattern and temperature field

Figure 2 shows the flow pattern and temperature field of two cases: P/H = 1.0 and P/H = 3.0 for e/H = 0.15, Re = 40,000, indicating the influence of the relative pitch of the fin. In Figure 2(a) and (c) there are two vortices situated in front of and behind the fin. For the case of P/H = 1.0 the two vortices take a very large part of the space between the fins. For P/H = 3.0 the part occupied by the vortices comparing with the whole pitch length is much smaller. The most of the interfin wall is covered with main body fluid. As P/H increases the

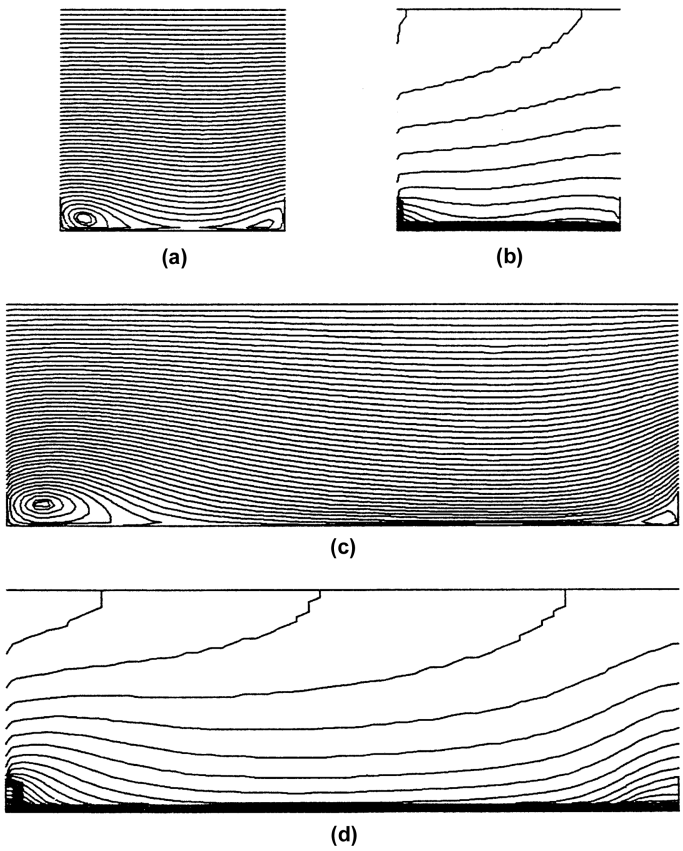

Figure 2.
Flow stream pattern and temperature field, e/H=0.15, Re=40,000, (a) and (b), P/H=1.0; (c) and (d), P/H=3.0

recirculating region at back of the fin becomes longer while the frontal vortex keeps nearly invariable. This is similar to that of the laminar flow in the channel with rod disturbances (Yuan and Tao, 1998). The common characteristic of Figure 2(b) and (d) is the concentricity of the isotherms near the wall. This quite differs from the results of laminar flow, indicating the great gradient of temperature in the vicinity of the wall and intensive heat transfer for turbulent flow.

Distribution of the local Nusselt number

Figure 3 shows the distributions of Nu(x) in the main flow direction for the cases of P/H=1.0, 3.0, 5.0 at e/H = 0.1 respectively. First we can see that for every case Nu(x) goes up largely when Reynolds number increases. Taking the case of P/H=1.0, e/H=0.1 as example, Nu_{max} varies from about 200 at $Re = 3 \times 10^4$ to about 400 at $Re = 7 \times 10^4$. At the same Reynolds number the Nu(x) for P/H=3.0 and 5.0 is higher than that of P/H=1.0. Different from the case of P/H=1.0, for case P/H=3.0 and 5.0 the Nu(x) curve possesses a minor peak in front of the fin in addition to the main peak at back of the fin. The minor peak of

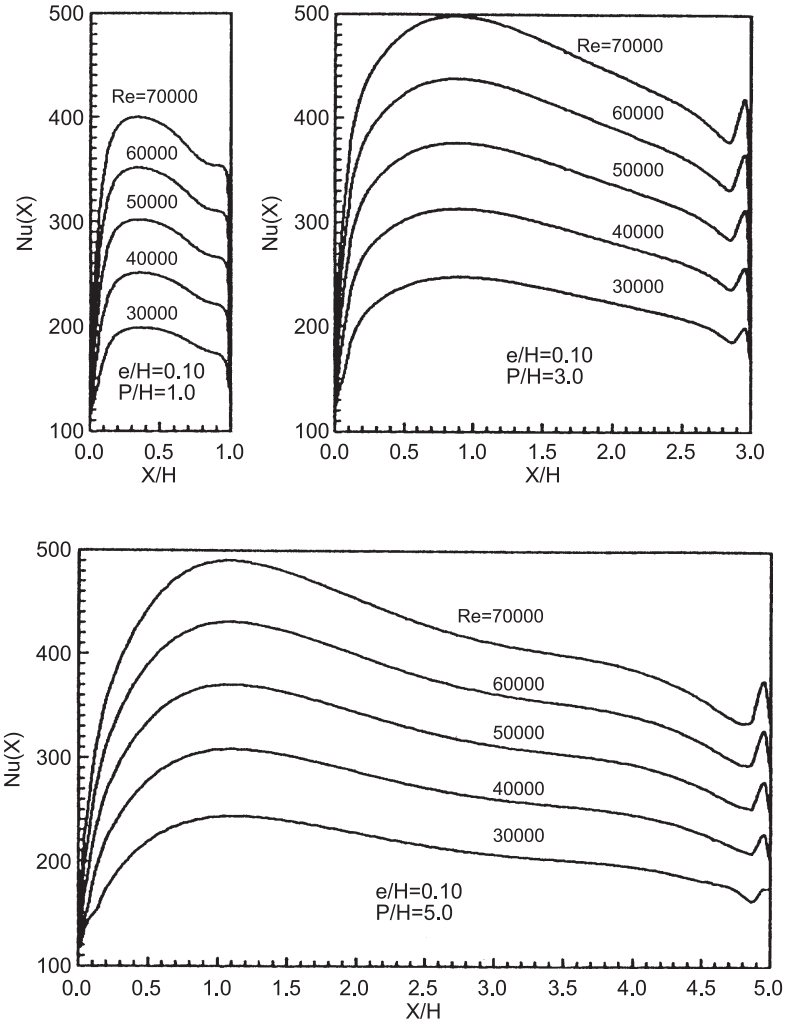

Figure 3.
Distributions of the local Nusselt number

Nu(x) becomes more apparent as Reynolds number increases. By analyzing the flow pattern in Figure 2 it can be seen that Nu_{max} corresponds approximately to the reattachment point at the back of the fin. From the reattachment point the flow in the wall-vicinity region divides into two paths: one goes along the main flow direction, another goes reverse upstream and forms the main vortex. This is similar to an oblique impingement jet onto a target plate, see Figure 4. At the reattachment point the Nu(x) reaches its maximum value. In both directions of upstream and downstream, apart from the peak, the Nu(x) declines gradually.

When the flow reaches near the next fin, there occurs a minor vortex in front of the fin because of the baffling function of it. The minor vortex rotates clockwise as the main vortex as shown in Figure 4. So the variation of the Nu(x) caused by the minor vortex is similar to that by the main vortex, i.e. there exists

a minor peak of Nu(x). The height of the peak is related to the intensity of the minor vortex. Figure 3 indicates that the minor peak locates in the site of a little distance from the fin. Within this distance the Nu(x) decreases sharply. Although the main vortex and the minor vortex rotate at the same direction, since they are in different wall corners, the main vortex in the right and the minor in the left, the heat transfer from the fin should be quite different for the front surface and the back surface when the fin kept different temperature from the fluid. To verify this inference and the influence of the thermal boundary condition of the fin to the heat transfer, a typical case, in which the fin surface is kept the same temperature as the main wall of the duct, has been simulated. Figure 5 shows the difference of Nu(Y) on the front and rear surface of the fin. Comparing with the rear surface curve, the front Nu(Y) not only possesses higher values but also changes largely. Chen and Huang (1991) also revealed this significance but for laminar flow. The Nu(x) distributions for both adiabatic and isothermal fin are shown in Figure 6. The two distributions are almost the same except for the little difference in the region before the fin. As to the Nu averaged by the fin pitch, the values are 273.7 for the adiabatic fin case

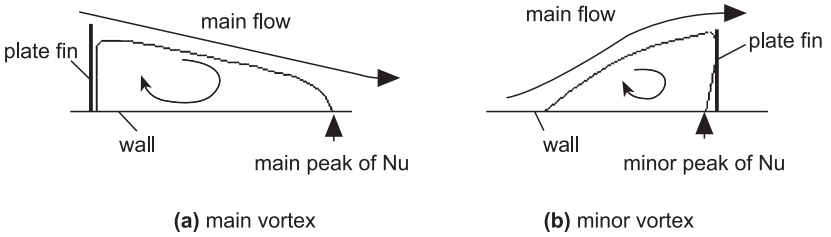

Figure 4.
Schematic diagram of the vortices and the peak of Nu(x)

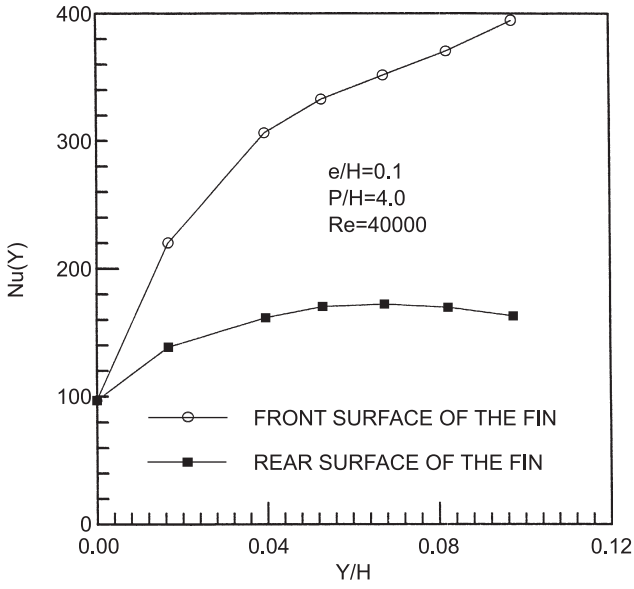

Figure 5.
Nu distribution on the fin surface

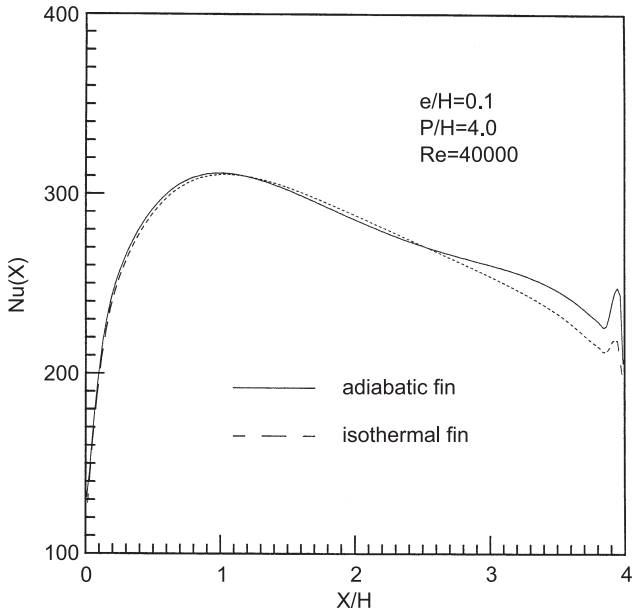

Figure 6.
Nu distributions on the main surface of the duct for different thermal boundary of the fin

and 294.5 for the isothermal fin case. They have a 7.6 percent relative difference. In the isothermal fin case the fin surface gives a contribution of 8.6 percent to the total Nusselt number.

With naphthalene sublimation technique, Sparrow and Tao studied the heat transfer in the narrow rectangular duct with rod disturbances. The obtained local Sherwood number, corresponding to the local Nusselt number, is shown in Figure 7(a). It can be seen that the distribution of the Sh in one cycle for the periodically fully developed region is similar to that of Nu(x) in Figure 3. In addition to the main peak of Sh there also exists some points of Sh near the rod that are apparently above the main undulating distribution curve. The authors considered that this phenomenon was caused by the intense but compact vortices lying in the front and back corner of the rod. By the present numerical results there exists a small vortex in front corner of the fin, which results in the minor peak of Nu(x) as discussed above. In the back corner there are not any vortices except the main one. Through detailed observation on the densely measured results of 640 points (see Figure 2 of Sparrow and Tao, 1983) it can be found that the higher Sh points deviating the main undulating distribution are all seemingly situated immediately fore of the rod, i.e. it is consistent with the present results. Myrum *et al.* (1993) studied the heat transfer enhancement in a ribbed duct with vortex generators experimentally. Though the performance was in the laminar flow ($Re \approx 3{,}450$), the profile of the Nu(x) obtained is also quite similar to the present numerical result, see Figure 7(b).

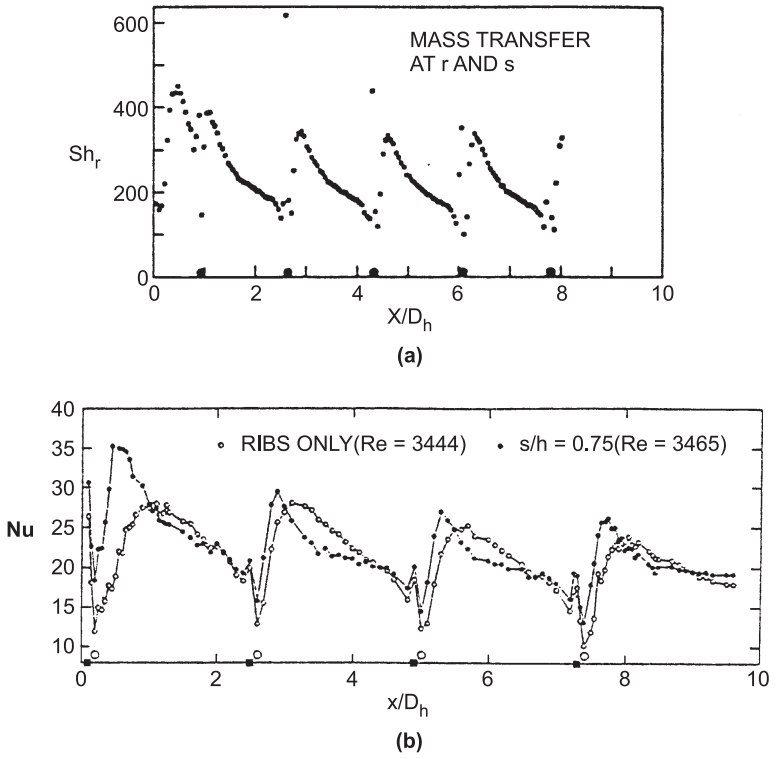

Figure 7.
Experimental result of the local Nusselt number (a) Sparrow and Tao (1983), e/H=0.082, P/e=28500, H is the duct height; (b) Myrum *et al.* (1993), e/H=0.104, P/e=38.4, Re=3,450

Effect of the pitch and height of the fin

For enhanced channels with various disturbances, the relative pitch, P/H, and the relative height, e/H, of the disturbances are most influential geometric parameters to the characteristics of the flow and heat transfer. Figure 8(a) presents the variations of the cycle-averaged Nusselt number, Nu, and friction factor, f, with P/H and e/H at the Reynolds number equal to 4×10^4. For a given e/H, Nu reaches its maximum at P/H=3.2. At the same Reynolds number for P/H values greater than 2.0, the higher the e/H, the higher the Nu in the range of the studied parameters. The situations for other Reynolds numbers are similar to this.

The changing tendency of f with P/H and e/H is shown in Figure 8(b). First, f increases with the increases of e/H for a given P/H, which is consistent with the usual results of enhanced channels (Chen and Huang, 1991; Sparrow and Tao, 1983). On the other hand, at the same e/H the change of f with P/H is relatively complex. For e/H=0.1 f drops monotonically with the increase of P/H, but when e/H is beyond 0.15 f has a maximum at P/H=2.0. This phenomenon may relate to the vortex change in the channels with higher disturbances.

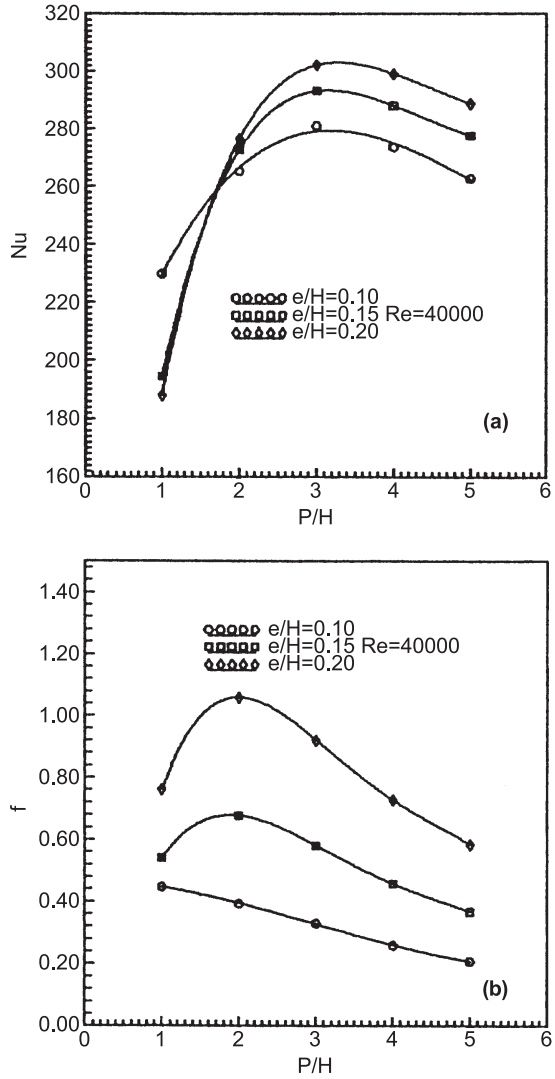

Figure 8.
Effect of the relative pitch and height of the fin to Nu and f

Relationship between Nu, f and Re

Attention is now turned to the discussion of the Reynolds number effect on the cycle-averaged characteristics. Figure 9 gives the relationship of Nu and Re for all studied cases. For purpose of comparison the curve of Dittus-Boelter equation for smooth duct has also been shown in the figure. It can be seen that for all cases Nu is higher than that of the smooth duct at the same Re. The rising extent of Nu over the smooth duct is not too much different for all cases except for the case of P/H=1.0. The ratio of Nu/Nu_o at the same Re is in the range of 2.7 to 3.2, with lower values for e/H=0.1 and higher values for e/H=0.2, while it changes little with the variation of Reynolds number.

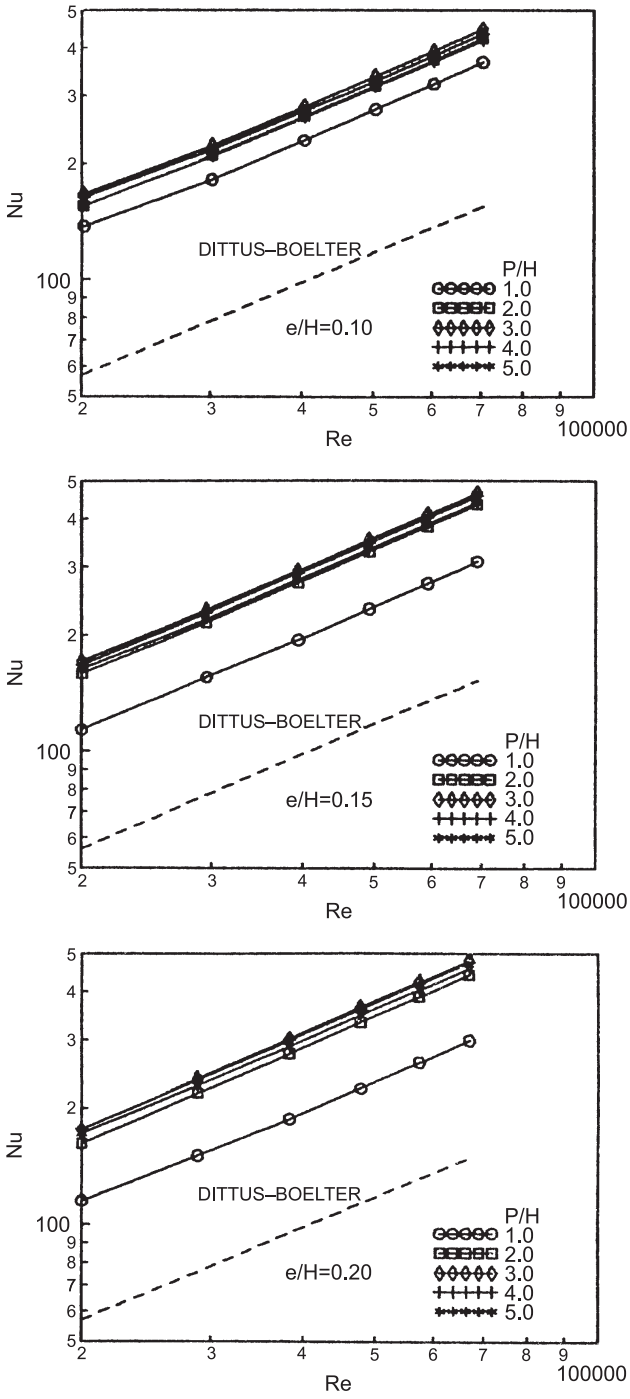

Figure 9.
Variation of cycle-averaged Nusselt number at different Reynolds numbers

In Figure 10 there are two aspects worthy of note about the relationship between f and Re. First, different from the situation of smooth duct's turbulent flow in which f gradually decreases with the increasing of Re (Blasius equation), the present results show that f is almost invariable with the Re, revealing typical characteristic of flow in "friction square region". By fluid mechanics the friction factor is only related with the roughness of the solid surface in the friction square region, but free of influence of Reynolds number. The second aspect is that f goes up largely comparing with f_o of smooth duct at the same Re. The value of f/f_o is from 8 to 50 approximately. Accompanying the enhancement of heat transfer the flow friction always rises, which is the common law for enhanced heat transfer channels (Sparrow and Tao, 1984; Yuan *et al.*, 1998). The further assessment about the enhanced effect of the studied configuration will be discussed in the following section. On the other hand, similar to the situation in Figure 9, f also increases with the e/H being higher. The difference between them is that the increasing extent of f is much bigger than Nu.

Performance assessment

As above mentioned, the Nu and f of the studied configuration both increase comparing with the smooth duct at the same Re. So it is necessary to find a method to evaluate the comprehensive augmented effect. There are different ways to attain this purpose. Here the assessment at the constraint condition of the same pump power is adopted.

The pump power for the fluid flow can be expressed as

$$N = \Delta p.(M/\rho) \tag{24}$$

where $\triangle$p is the pressure drop, M is the mass flow and ρ is the density. The constraint condition for the same pump power is

$$N = N_o \tag{25}$$

indicating the power consumption of the enhanced configuration is equal to that of the smooth duct. Assuming the geometric dimensions of both ducts and the thermophysical properties of the fluid are the same, the following equation can be derived from equation (25)

$$f\mathrm{Re}^3 = f_o\mathrm{Re}_o^3 \tag{26}$$

The relationship of f_o and Re_o can be determined by Blasius equation

$$f_o = 0.3164\mathrm{Re}_o^{-0.25} \tag{27}$$

while the friction factor of the enhanced duct can be written as

$$f = 0.3164(\frac{f}{f_o})_{\mathrm{Re}}.\mathrm{Re}^{-0.25} \tag{28}$$

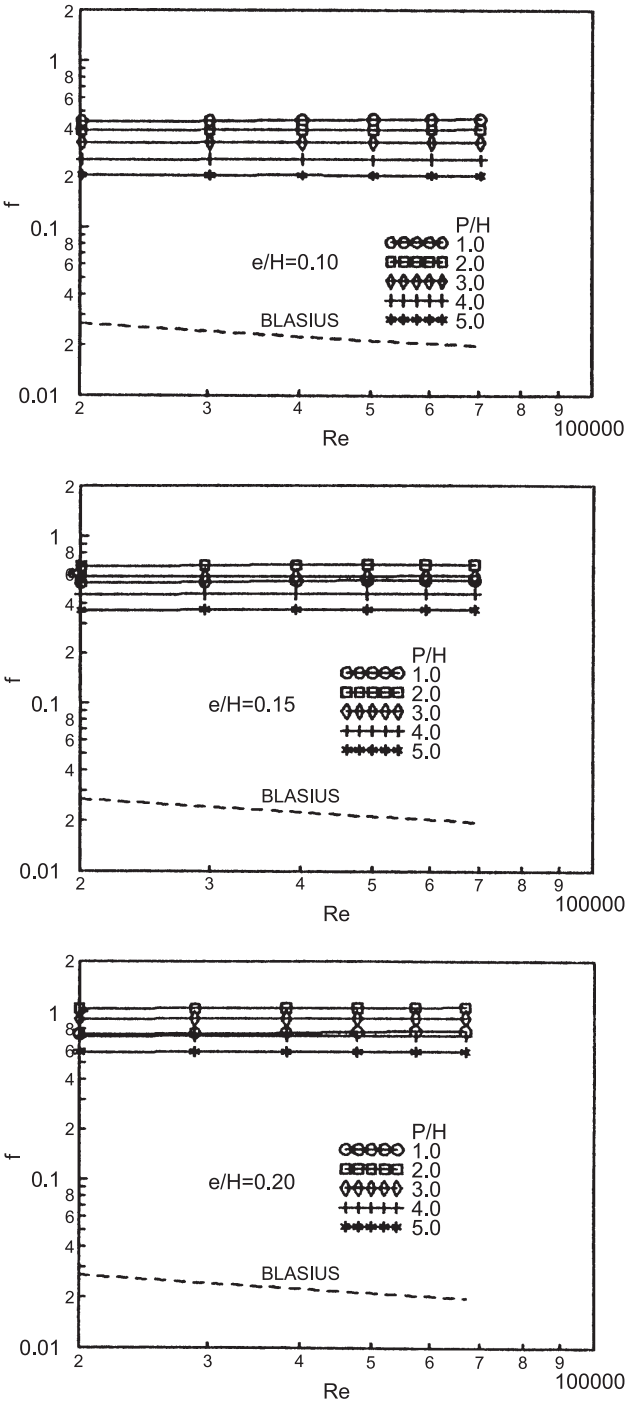

Figure 10.
Variation of cycle-averaged friction factor at different Reynolds numbers

Divide equation (28) by equation (27) we obtain

$$\frac{f}{f_o} = (\frac{f}{f_o})_{\mathrm{Re}} \cdot (\frac{\mathrm{Re}}{\mathrm{Re}_o})^{-0.25} \tag{29}$$

Substitute equation (26) into above equation, there is

$$\frac{\mathrm{Re}}{\mathrm{Re}_o} = (\frac{f}{f_o})_{\mathrm{Re}}^{-0.3636} \tag{30}$$

This is the relationship of Re and Re_o at the constraint condition of the same pump power. The $(f/f_o)_{Re}$ in the equation is determined by the numerical f value and the f_o value calculated from Blasius equation, as shown in Figure 10.

Now the Nusselt numbers corresponding to Re and Re_o can be determined respectively. The Nu is from the numerical results and the Nu_o is by the Dittus-Boelter equation. Then the ratio indicating the net enhancement of the studied configuration, Nu/Nu_o, is obtained. The Nu/Nu_o at different Reynolds numbers for the 15 cases are shown in Figure 11. For a given fin height Nu/Nu_o goes up when P/H increases in the studied range of parameters. This suggests that the disturbances must be deployed properly. Too dense fins probably cause the net enhancement to degrade, i.e. $Nu/Nu_o<1$. On the other hand, too big P/H is also unsuitable to get notable effect of enhancement. From Figure 11 we can see that though Nu/Nu_o becomes higher with the P/H increase, the rate is more and more slow. It can be inferred that at some bigger P/H value the Nu/Nu_o starts to go down with the P/H increase further, which means that there exists a maximum of Nu/Nu_o. Comparing the results of e/H = 0.10, 0.15 and 0.20 it is found that the effect of e/H = 0.10 is the best. The bigger the e/H, the less the net enhancement. If we take $Nu/Nu_o>1.1$ as the judging standard, the efficient parameters for the studied configuration is as

$$\begin{aligned} \mathrm{e/H} &= 0.10, \qquad \mathrm{P/H} \geq 2 \\ \mathrm{e/H} &= 0.15, \qquad \mathrm{P/H} \geq 3 \\ \mathrm{e/H} &= 0.20, \qquad \mathrm{P/H} \geq 4 \end{aligned}$$

For every case Nu/Nu_o decreases with Re increasing, while the change rate is quick for $Re<3 \times 10^4$ and slow for $Re>3 \times 10^4$.

There are some similarities between the results of the present investigation and that of the ducts with rod disturbances studied by Sparrow and Tao (1984). In their results, when the relative height of the rod, e/(H/2), is equal to 0.164 and the relative pitch, P/(H/2), equal to 3-12 (H representing the height of the duct, different from the present study), there is $Nu/Nu_o>1$. But for e/(H/2) equal to 0.328 and the same P/(H/2) as above there are cases of $Nu/Nu_o<1$ at higher Reynolds numbers, indicating the degradation of heat transfer. The maximum of Nu/Nuo for the rod-ribbed duct is about 1.5 while it is 1.6 for the present configuration.

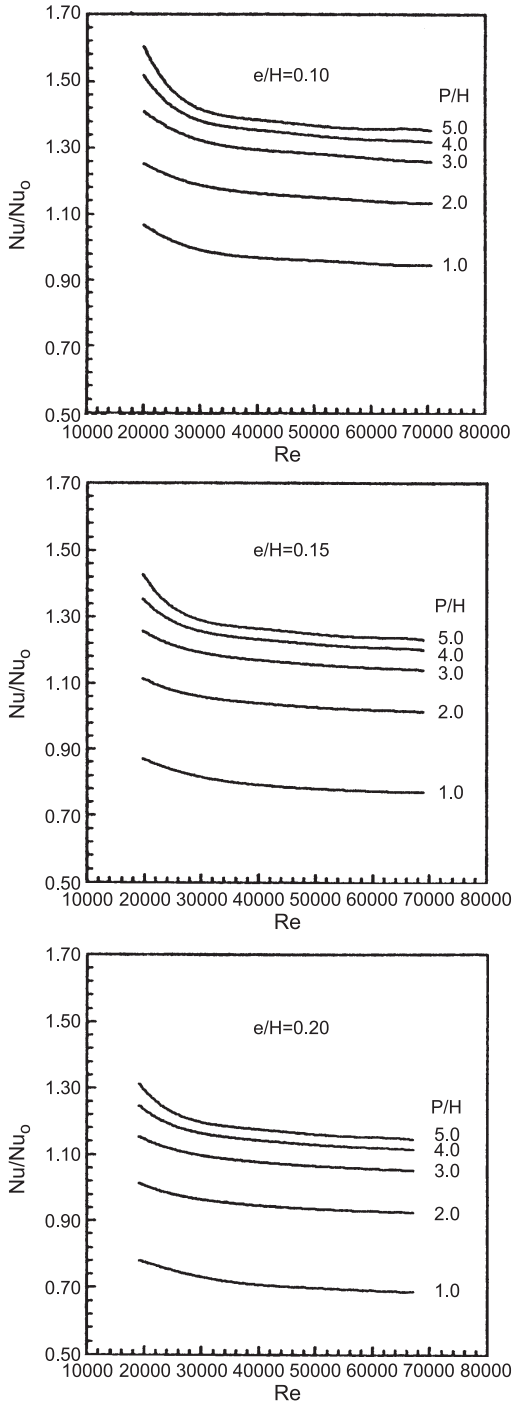

Figure 11.
Performance assessment on the enhanced channel at the same pump power

Check the steady results with transient algorithm

Considering the bifurcation of flow in some cases in which the steady boundary conditions are kept (Durst *et al.*, 1993), it is necessary to check the above steady results using the transient governing equations. If the transient result converges to the solution of the steady governing equations when the time approaches infinity, the validity of the steady algorithm is verified. For this purpose some cases with big fin height (e/H = 0.2) have been checked using transient algorithm. The result of the case of P/H = 4.0, Re = 40,000 are shown here. Figure 12 shows the curve of the averaged Nu changing with the iterative time step. We can see that after one peak Nu converges to a steady value that is consistent with the result of steady case very well. The difference between the two cases is about 1.7 percent for the friction factor and 1.2 percent for the averaged Nusselt number.

Figure 13 gives the Nu distributions at four iterative times. After 140 seconds of iteration the Nu(X) increases with the time monotonically. When the time equals to 1,200s the distribution of Nu(X) reaches its final shape approximately. This corresponds to the change of the Nu curve in Figure 12.

By the checking results of the transient algorithm, the steady governing equations are valid for the simulation of this studied enhanced configuration.

Concluding remarks

The parallel-plate channel with periodic transverse fins has been numerically investigated thoroughly to determine its characteristics of turbulent flow and heat transfer. The K-ε turbulent model and wall function to deal with the variables in the vicinity of the solid wall have been adopted in the study. The flow stream pattern in a cycle shows that there exists two vortices situated immediately fore and aft of the fin. The aft vortex is apparently longer than the fore one. With the increase of the fin pitch and height the aft vortex becomes longer while the fore one keeps almost invariable.

The local Nusselt numbers along the main flow direction have been obtained for different geometric parameters of the fin in the range of $Re = 2 \times {}^{10} - 7 \times 10^4$.

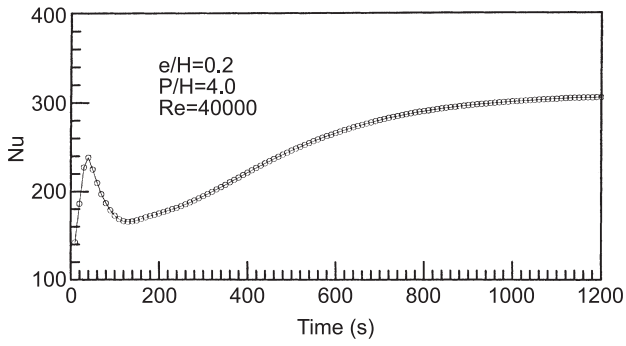

Figure 12.
The averaged Nu along the main surface of the duct changes with the time step when the transient algorithm is employed. The fin is adiabatic

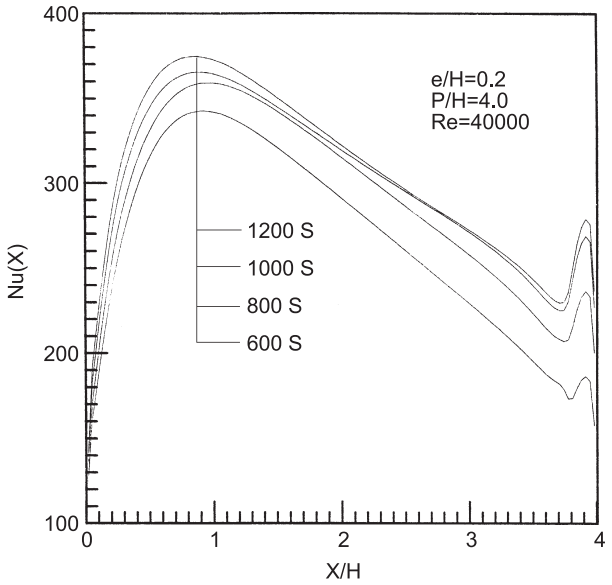

Figure 13.
Nu distributions changing with the time step when the transient algorithm is employed, while the fin is kept adiabatic

The distribution of Nu(x) reveals that there is a minor peak in the front vicinity of the fin in addition to the main one generated by the aft vortex. The cycle-averaged friction factor and Nusselt number is also analyzed.

Finally, the assessment about the enhanced heat transfer at the constraint of the same pump power is conducted. The results indicate that the effect for e/H=0.10 is superior to those for e/H=0.15 and 0.20. Properly enlarging the fin pitch is profitable to both the heat transfer enhancement and the frictional reduction. The comparison between the studied configuration and the ducts with periodic rod disturbances shows that the two kinds of ducts keep almost the same maximum of net enhancement of heat transfer.

To assure the validity of the steady algorithm for the present study the transient governing equations are also employed to check the results of the steady solution. The results from the two different algorithms are highly consistent with each other.

References

Amano, R.S. (1985), "A numerical study of laminar and turbulent heat transfer in a periodically corrugated wall channel", *ASME J. Heat Transfer*, Vol. 107, pp. 564-9.

Amano, R.S., Herlee, A.B., Smith, R.J. and Niss, T.G. (1987), "Turbulent heat transfer in a corrugated-wall channel with and without fins," *ASME J. Heat Transfer*, Vol. 109, pp. 62-7.

Chen, C.H. and Huang, W.H. (1991), "Prediction for laminar forced convection in parallel-plate channels with transverse fin arrays", *Int. J. Heat Mass Transfer*, Vol. 34 No. 11, pp. 2739-49.

Chieng, C.C. and Launder, B.E. (1980), "On the calculation of turbulent heat transport downstream from an abrupt pipe expansion", *Numerical Heat Transfer*, Vol. 3, pp. 189-207.

Durst, F., Pereira, J.C.F. and Tropea, C. (1993), "The plane symmetric sudden-expansion flow at low Reynolds numbers", *J. Fluid Mechanics*, Vol. 248, pp. 567-81.

Farouk, B. and Guceri, S.I. (1982), "Laminar and turbulent natural convection in the annulus between horizontal concentric cylinders", *ASME J. Heat Transfer*, Vol. 104, pp. 631-6.

Hong, Y.J., Hsieh, S.S. and Shih, H.J. (1991), "Numerical computation of laminar separation and reattachment of flow over surface-mounted ribs", *ASME J. Fluids Engineering*, Vol. 113, pp. 190-8.

Launder, B.E. and Spalding, D.B. (1974), "The numerical computation of turbulent flows, computer methods in applied mechanics and engineering", Vol. 3, pp. 269-89.

Myrum, T.A., Qiu, X. and Acharya, S. (1993), "Heat transfer enhancement in a ribbed duct using vortex generators", *Int. J. Heat Mass Transfer*, Vol. 36 No. 14, pp. 3497-508.

Patankar, S.V. (1981), "A calculation procedure for two-dimensional elliptic situations", *Numerical Heat Transfer*, Vol. 4, pp. 405-25.

Pourahmadi, F. and Humphrey, J.A.C. (1983), "Prediction of curved channel flow with an extended K-ε model of turbulence", *AIAA J.*, Vol. 21, pp. 1365-73.

Serag-Eldin, M.A. and Spalding, D.B. (1979), "Computations of three dimensional gas turbine combustion chamber flows", *ASME J. Engineering Power*, Vol. 101, pp. 327-36.

Sparrow, E.M. and Tao, W.Q. (1983), "Enhanced heat transfer in a flat rectangular duct with streamwise-periodic disturbances at one principle wall", *ASME J. Heat Transfer*, Vol. 105, pp. 851-61.

Sparrow, E.M. and Tao, W.Q. (1984), "Symmetric vs asymmetric periodic disturbances at the walls of a heated flow passage", *Int. J. Heat Mass Transfer*, Vol. 27 No. 11, pp. 2133-44.

Xin, R.C. and Tao, W.Q. (1988), "Numerical prediction of laminar flow and heat transfer in wavy channels of uniform cross-sectional area", *Numerical Heat Transfer*, Vol. 14, pp. 465-81.

Yuan, Z.X. and Tao, W.Q. (1998), "Numerical prediction for laminar forced convection heat transfer in parallel-plate channels with streamwise-periodic rod disturbances", *Int. J. Numerical Methods in Fluids*, Vol. 28, pp. 1371-87.

Yuan, Z.X., Tao, W.Q. and Wang, Q.W. (1999), "Experimental investigation of heat transfer enhancement in ducts with winglet fins", *Pro. First Int. Conference of Engineering Thermophysics*, 21-23 August, Beijing, China, pp. 457-63.

Yuan, Z.X., Wang, Q.W. and Tao, W.Q. (1998), "Experimental study of enhanced heat transfer in ducts with periodic rectangular fins along the main flow direction", *Pro. 11th IHTC*, 23-28 August, Kyongju, Korea, Vol. 5, pp. 327-32.